Supplementary Information

Understanding the catalyst-free transformation of amorphous carbon into graphene by current-induced annealing

Amelia Barreiro*[,†,1], Felix Börrnert*[,†,2], Stanislav M. Avdoshenko[3,4], Bernd Rellinghaus[2], Gianaurelio Cuniberti[3], Mark H. Rümmeli[2,3], Lieven M. K. Vandersypen[1]

[†] both authors contributed equally

[1] Kavli Institute of Nanoscience, Delft University of Technology, Lorentzweg 1, 2628 CJ Delft, The Netherlands

[2] IFW Dresden, Postfach 270116, 01171 Dresden, Germany

[3] TU Dresden, 01062 Dresden, Germany

[4] School of Materials Engineering, Purdue University, West Lafayette, IN, USA

Section 1. Experimental methods

We have performed in-situ transmission electron microscopy (TEM) studies of graphene growth from a-C by current-induced annealing. In order to observe the dynamics of these structural changes the chip with the contacted graphene sample was mounted on a custom-built sample holder for TEM with electric terminals, enabling simultaneous TEM imaging and electrical measurements. For imaging, a FEI Titan[3] 80–300 TEM with a CEOS third-order spherical aberration corrector for the objective lens was used. It operated at an acceleration voltage of 80 kV to reduce knock-on damage. The images were recorded with a Gatan UltraScan 1000 camera via the Gatan DigitalMicrograph software. To enhance the temporal resolution for in situ observation down to 350 ms per frame the camera was used in conjunction with the TechSmith Camtasia Studio screen recorder software at 4 pixel binning with an acquisition time of 0.05 s.

Section 2. Preferential deposition of a-C on the edges of individual layers and defects in few layer graphene

The source of a-C can originate from the decomposition of hydrocarbons in the TEM column and/or from hydrocarbon-containing organic impurities adsorbed on the chip, the chip carrier and the sample holder. The mobile hydrocarbons diffuse and reach the area exposed to the electron beam. Under electron irradiation at 80 kV, mobile hydrocarbon deposits are converted to a-C, while hydrogen atoms are knocked out by electron impacts. We observed on 3 samples that preferential sites for a-C adsorbtion and consequent a-C formation are edges or defect sites of few layer graphene, see "Fig. S1". A possible explanation for this finding is that during the diffusion of the mobile hydrocarbons on the graphene surface, they encounter an obstacle when reaching an edge or a defect and tend to adsorb there. As a result, a-C deposits form and gradually grow bigger.

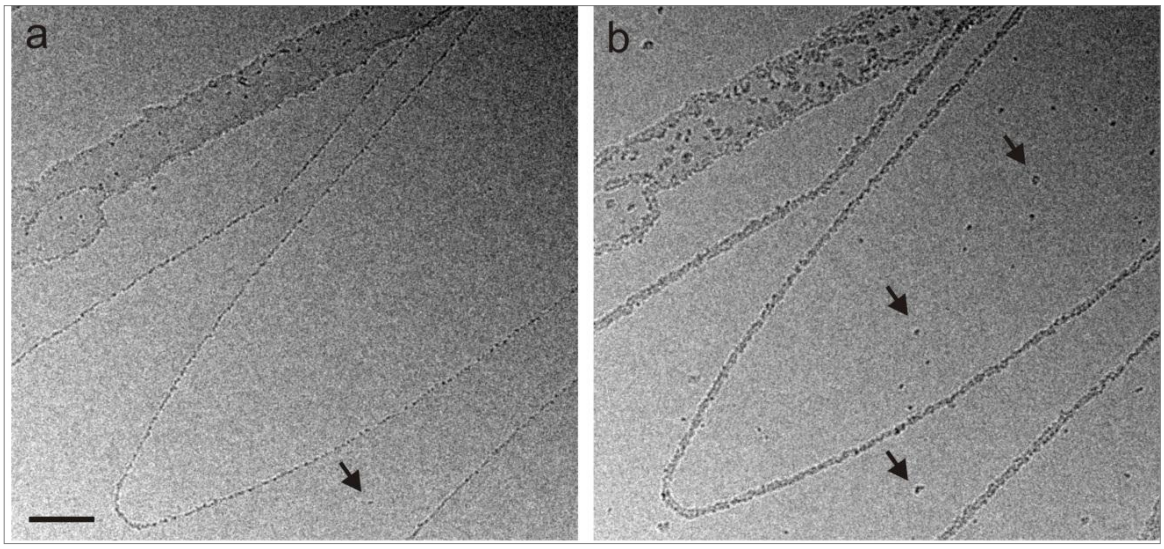

Figure S1. TEM images of the stepwise deposition of a-C. (a,b) At the edges of the individual layers in few layer graphene flakes and (b) other defects. The arrows point at defects in the lattice where a-C agglomerates while the continuous lines with elliptical shapes separate regions with a different number of layers. a-C preferentially deposits at the step edges. The scale bar is 50 nm.

Section 3. Effect of the 80 keV electron beam

In all the experiments we image with an 80 keV beam. It has been reported that an 80 keV beam can lead to the healing of multivacancies with up to 20 missing atoms by lattice reconstructions [1]. Nevertheless, for free-standing graphene, the electron beam can only heat up the sample in the order of about 1 K [2]. In contrast, current annealing in the high current limit was estimated to lead to temperatures as high as 2000 - 3000 °C [3-5]. Therefore, the main driving mechanism to the formation of graphene from a-C should originate from Joule heating, although we cannot exclude that there might be a contribution to the transformation from the electron beam. Indeed, the electron beam does induce crystallization of the amorphous carbon [6], but the time scale of the conversion is about one order of magnitude slower.

Importantly, if TEM imaging was performed without concomitant current annealing we never observed the formation of graphene out of a-C but only the deposition of increasing quantities of a-C. Moreover, if as-fabricated graphene flakes are imaged without a previous current annealing step, residues from fabrication react with the graphene by beam-driven chemical modifications with contaminants and adsorbates at energies below the knock-on threshold [7] leading to the rupture of the flakes, see "Fig. S2".

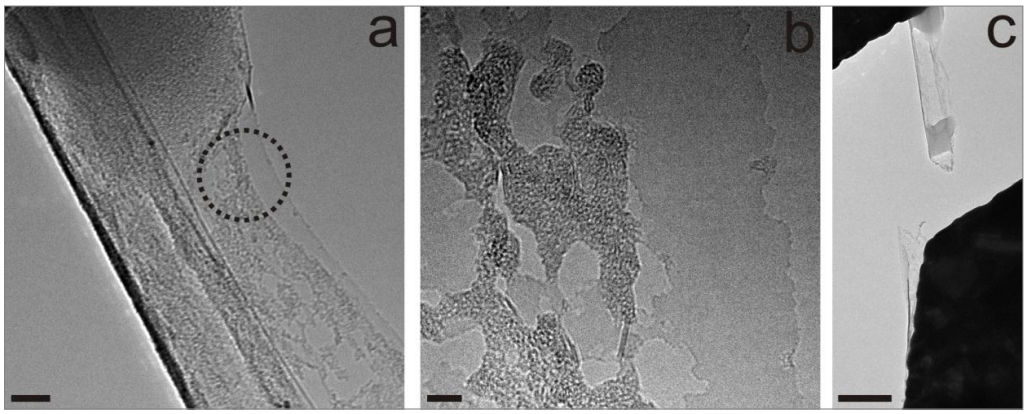

Figure S2. Effect of the 80 keV beam. (a) TEM image of a few-layer graphene flake contaminated by fabrication residues. The scale bar is 20 nm. (b) Hole formation due to beam-driven chemical modifications in the lattice with the contaminants. The scale bar is 5 nm. (c) Rupture of the graphene due to an excessive accumulation of holes. The scale bar is 200 nm.

Section 4. Transformation of a-C to graphene

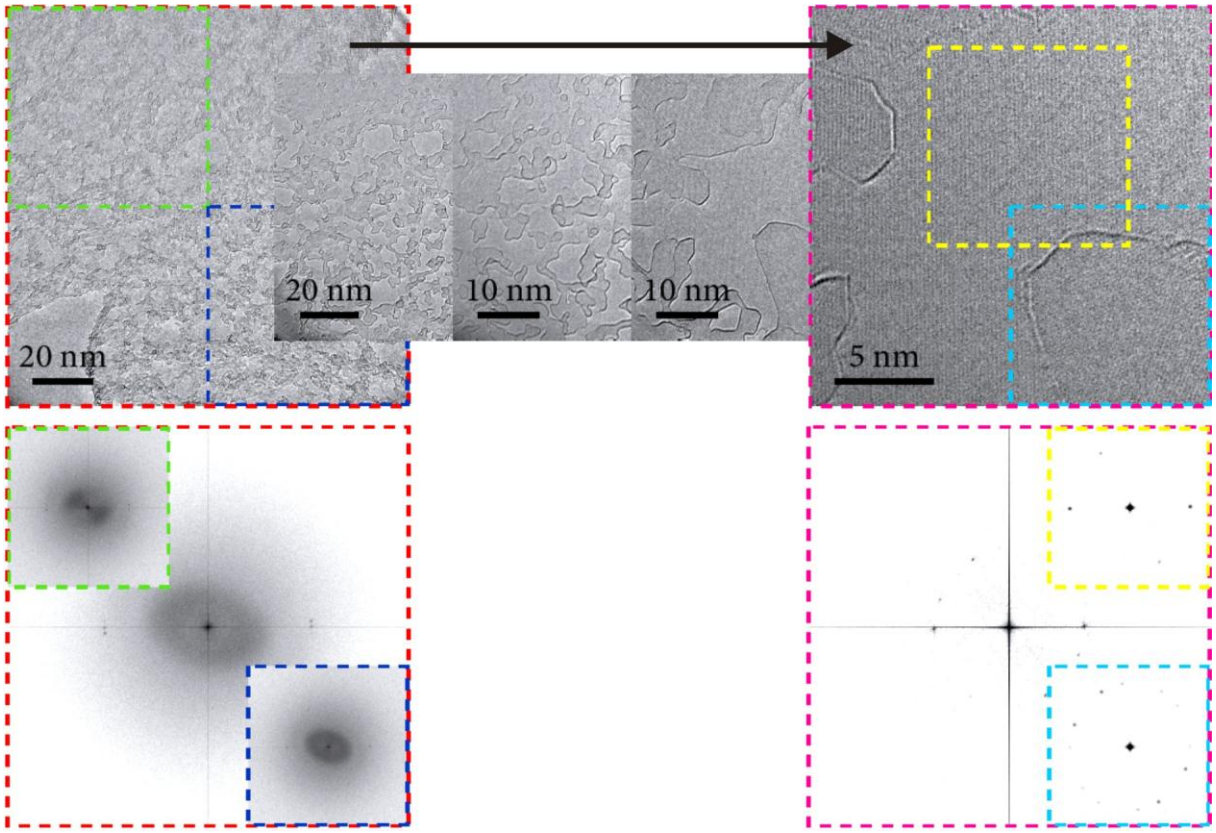

Figure S3. Transformation of a-C into graphene. Upper panel. TEM images of the stepwise transformation of a-C into graphene patches by means of current annealing. The black arrow indicates their sequence in time. The first (big) micrograph on the left was formed by two deparated pieces of graphene that fused together [8]. Moreover, both of them are covered with a-C.

Lower panel. Corresponding Fourier Transforms (FT) of the first and last (big) TEM micrographs in the upper panel. (Left) The two separate graphene pieces that fused lead to two FT patterns – one for each side. The big image corresponds to the FT transform of the complete micrograph, while the two smaller ones correspond to the regions marked by the green and blue squares in the separated layers. (Right) The big image corresponds to the FT transform of the complete micrograph, while the two smaller ones correspond to the regions marked by the yellow and orange squares. In the region marked by the orange square we can observe the „original“ graphene FT pattern of the lower flake, while in the region marked by the yellow square we can distinguish an additional FT pattern arising from the newly grown graphene patch. The newly grown graphene patch has a different orientation as compared to both of the initial graphene flakes.

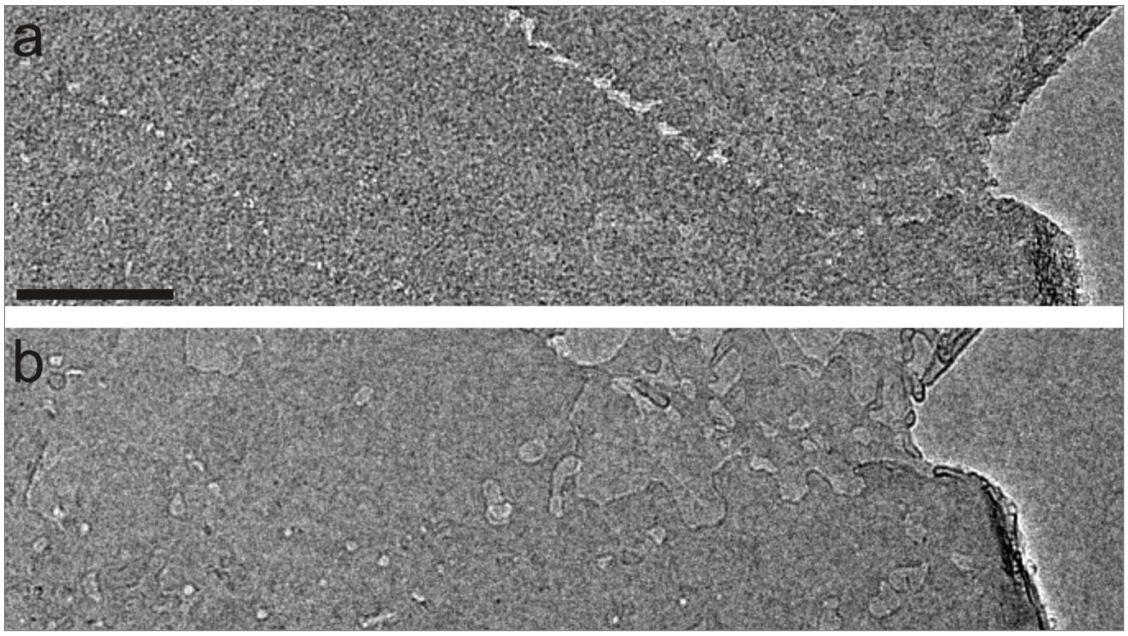

Figure S4. Overview of the transformation of a-C into graphene. (a) TEM image of a-C on graphene. The scale bar is 50 nm. (b) TEM image of a layer of graphene grown from a-C that is more than 100 x 300 nm in size and only contains few defects, showing that this process could be scalable.

Section 5. Healing of holes

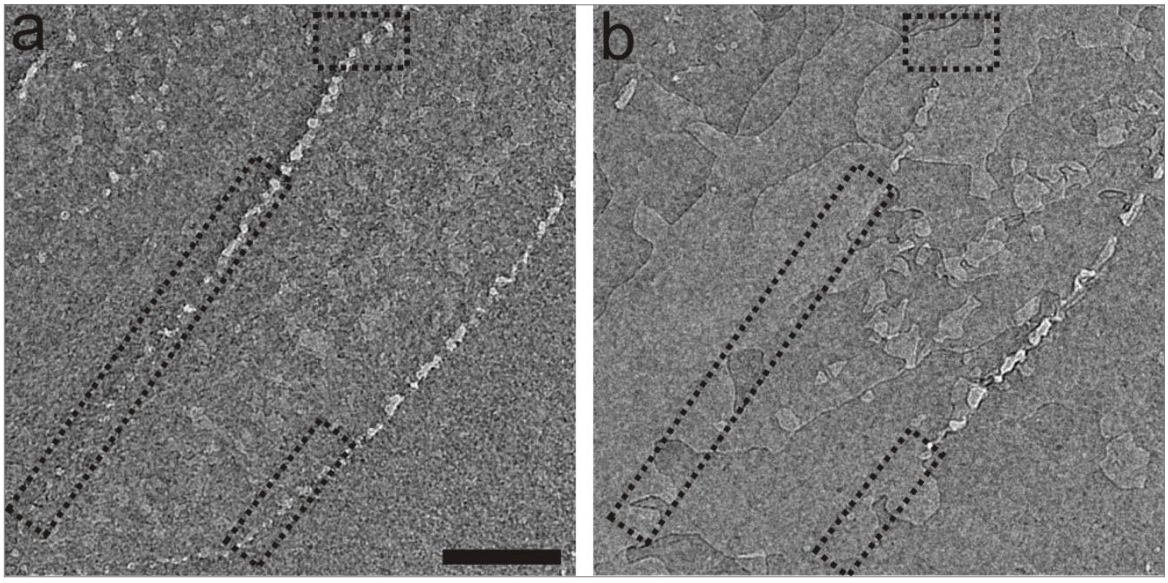

Figure S5. TEM images of the gradual healing of holes (bright spots) in the few-layer graphene terraces by means of current annealing in the presence of a-C at 3 V, 0.9 mA. The dotted boxes enclose regions where holes healed out. The scale bar is 50 nm. The time elapsed between (a) and (d) is 3min 30s.

Section 6. Molecular Dynamics Simulations

We conducted a series of molecular dynamics (MD) simulations to gain further insight into our experimental findings regarding, first, the transformation of a-C to graphene at high temperatures on top of a graphene substrate and, second, on the healing of holes in a graphene lattice at high temperatures with an a-C feedstock.

Born-Oppenheimer G-point molecular dynamics with the non-consistent charge (NCC) - density functional tight-binding (DFTB) scheme [9] were performed. A canonical Nosé-Hoover constrained (NVT) ensemble with a 300 K bath temperature and Nosé-Hoover chains with 100 fs coupling rate were used for initial equilibration (20 ps). The stability of the system was then studied by means of heating steps. Minor deviations between the NCC- and self-consistent charge (SCC) – DFTB [10] results found during the initial equilibration at 300 K justified the use of NCC-DFTB method for all further studies. A standard van der Waals term was included in our DFTB scheme by fitting the London dispersion formula [11]. The system's parameterization for a classical guess was done based on the Tersoff theory [12]. The dynamical trajectories are described by a classical Lagrangian with an isothermal constraint condition given by the Nosé-Hoover theory [13] applied to a system containing N particles, a velocity Verlet integrator, using a time step of 1 fs (100 fs coupling rate and 3 chains). Trajectory analysis was done using the Visual Molecular Dynamics (VMD) interface [14].

6.1 Transformation of a-C to graphene

In the experiments, the graphene that acts as a substrate heats up to very high temperatures due to current-induced annealing. The temperatures achieved were estimated to be around 2000 - 3000 ºC [2, 3, 4]. To reproduce this situation in the theoretical modeling we assume a canonical ensemble as the heat source for the whole system at a constant temperature. We conducted MD simulations employing module DFTB embedded in a CP2k package [15] of a perfect 30x30 A^2 graphene substrate and four a-C clusters of 1 nm diameter on top. These a-C clusters are arranged in tetragonal packing on top of the graphene substrate at a distance of ~ 3.5 Å.

We first turn to the simulation of the clusters of a-C. According to P.W. Anderson [16] a-C is restricted to the description of carbon materials with a localized π-electron system, and in each particular case the sp^2/sp^3 ratio should be specified explicitly. In our experiments, the sp^2/sp^3 ratio cannot be determined experimentally and we modeled it to be 50/50. Each isolated cluster with randomly chosen atomic coordinates satisfying this ratio was first annealed using the non-bonded potential given by Tersoff theory [12] coupled to 300 K NVT (Nosé-Hoover constrain, 3 chains, 100 fs coupling).

During the MD simulations, the 30x30 $Å^2$ graphene substrate and the four a-C clusters on top are subject to stepwise increasing temperatures. In particular we chose 300, 600, 1200 and 1800 K. The temperatures in the simulations are achieved by a Nosé-Hoover (NH) thermostat [13] with 15 ps annealing at each step, in the frame of the NCC-DFTB model. In the simulations the next temperature step was applied when the potential energy per atom of the a-C cluster subsystem didn't change significantly on the time frame of 2 ps and no more structural changes occurred at that temperature because there is a local minimum of the relative potential energy per carbon atom of the a-C. We used the stepwise annealing strategy to slowly overcome

these energy barriers by means of the energy flux provided by the thermostat. The simulations were reproduced 5 times starting with the same geometry but with different initial velocities. A representative example of the stepwise annealing and the corresponding structural changes of the a-C are shown in "Figure S6". Upon increasing temperature, the a-C begins to transform, goes through a glasslike phase and finally forms a graphene lattice. Notably, whereas in the range between 600 and 1200 K the elements produced from the initial a-C clusters remain separated from each other, at 1800 K the elements start to self-assemble and finally produce a single graphene flake. The structure formed is flat and is located 3.5 A above the initial graphene template, similar to the graphite interlayer distance. However, the top crystallographic orientation of the top layer is not aligned with that of the bottom layer, similar to what we observe in the experiments.

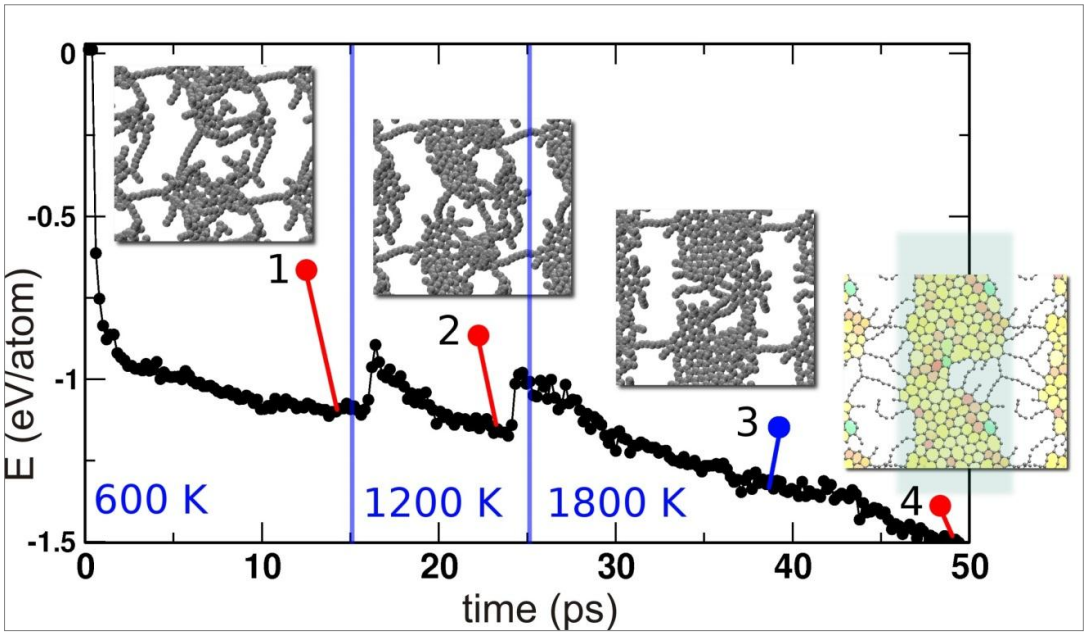

Figure S6. MD simulations illustrating the stepwise transformation of a-C to graphene at different temperatures. Potential energy changes of the a-C subsystem for a representable run. Insets 1-4 represent on-time geometries for t = 12.5, 24, 38 and 49 ps, respectively.

When the initially well-equilibrated system at 300 K was directly coupled to a thermostat at 1200 – 1800 K (with 100 fs coupling rate, with integration step 1 fs among the trajectory) in one step, it resulted in an overheating of the a-C and carbon dimer cloud formation leading to an explosion. After such an event, the system required a long time to return back into a compact structure.

However, if the thermal energy is supplied step by step (300, 600, 1200 and finally 1800 K) the system, consisting of the graphene substrate and the 4 a-C clusters on top, remains compact and only internal quick transformations and rearrangements occur. Keeping the system for a long time at 300 K leads to the formation of long fibers, without many changes in a time span of about 10.0 ps. After drastic and quick changes during the first 2 ps the a-C transformation is relaxed to a "glass" form (a local minima) where it stays constant, see "Figure S6 inset 1". This can be understood in terms of the relative energy of the a-C fragment reaching a plateau after several picoseconds of annealing.

Raising the temperature to 1200 K leads initially again to quick rearrangements. The elements distributed over isolated islands are reminiscent of conjugated cage-like structures and are topologically close to a

polyaromatic system, "see Figure S6 panel 2". Nevertheless, again the transformation slows down after several ps.

After the next temperature step to 1800 K, the system evolves faster, as can be seen from the increased potential energy slope, "see Figure S-6 (panels 3 and 4)" until graphene is formed which sticks at a distance of 3.5 A to the graphene template. Introducing additional amounts of a-C helps to heal long defects out, as all the a-C initially introduced is not available anymore to be integrated into the forming graphene lattice.

These MD simulations nicely illustrate the role of our graphene template, which prevents the formation of fullerene- like structures.

6.2 Healing of holes in graphene at high temperatures

We simulated a hole of 1 nm radius in an ideal graphene flake and placed 3 a-C clusters (1 nm^3) on top of it. In total we followed 5 independent trajectories with different structures and initial velocities. For all these independent MD runs we observed that the hole is healed completely but contains at least one Stone-Wales defect [17], "see figure S7". The formation of Stone-Wales defects is promoted by radicals in a reaction atmosphere [18]. Once these defects are formed, they are extremely stable and an energy of about 4.6 – 7 eV [19, 20] is required to transform the defect to hexagonal sp^2 bonds. During the MD runs it will be very rare to reach such high energies during a time span of 30 ps such as in our calculations. Much longer timescales are not feasible from a computational point of view. Nevertheless, it seems that in the real experiment, Stone-Wales defects are healed out during the rather long experiment time.

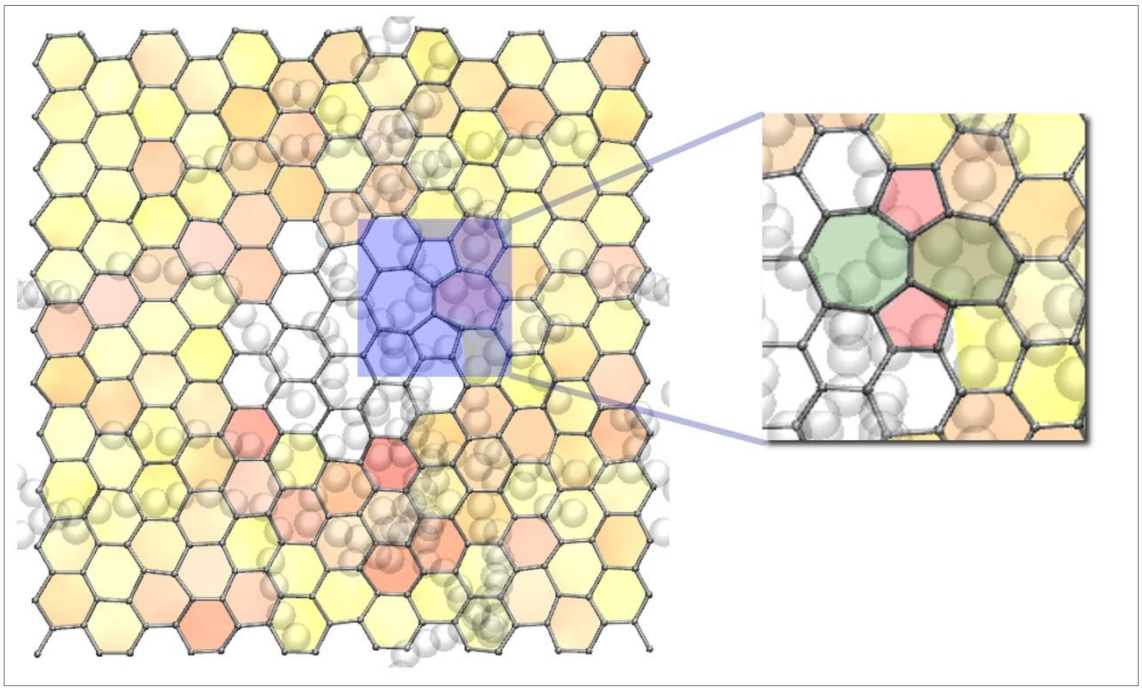

Figure S7. Molecular dynamics simulations at 1800 K showing the repaired hole in figure 8. Zoom-in into a Stone-Wales defect. The colors represent the actual number of vertices of the rings and their bending order. The full color code is described in Table 1 on page 134 in Ref. 21.

References

[1] Börrnert, F.; Gorantla, S.; Bachmatiuk, A.; Warner, J. H.; Ibrahim, I.; Thomas, J.; Gemming, T.; Eckert, J.; Cuniberti, G.; Büchner, B.; Rümmeli, M. H. Phys. Rev. B 2010, *81*, 201401R.
[2] Egerton, R.; Li, P.; Malac, M. Micron 2004, 35, 399-409.
[3] Huang, J. Y.; Ding, F.; Yacobson, B. I.; Lu, P.; Qi, L.; Li, J. Proc. Natl. Acad. Sci. USA 2009, *106*, 10103 – 10108.
[4] Huang, J. Y.; Chen, S.; Ren, Z. F.; Chen, G.; Dresselhaus M. S. NanoLett. 2006, *6*, 1699-175.
[5] Asaka, K.; Karita, M.; Saito, Y. Appl. Phys. Lett. 2011, *99*, 091907.
[6] Bo̎rrnert, F.; Avdoshenko, S. M.; Bachmatiuk, A.; Ibrahim, I.; Bu̎chner, B.; Cuniberti, G.; Ru̎mmeli, M. Adv. Mater. 2012, 24, 5630−5635.
[7] Warner, J. H.; Schäffel, F.; Zhong, G.; Rümmeli, M. H.; Büchner, B.; Robertson, J.; Briggs, A. D. ACS Nano 2009, *3*, 1557-1661.
[8] Barreiro, A.; Börrnert, F.; Rümmeli, M. H.; Büchner, B.; Vandersypen, L. M. K. Nano Lett. 2012, *12*, 1873-1878.
[9] Porezag, D.; Frauenheim, T.; Köhler, T.; Seifert, G.; Kaschner, R. Phys. Rev. B 1995, *51*, 12947.
[10] Seifert, G.; Porezag, D.; Frauenheim, T. Int. J. Quantum Chemistry 1996, *58*, 185-192.
[11] Elstner M.; Hobza, P.; Frauenheim, T.; Suhai, S.; Kaxiras, E. J. of Chem. Phys. 2001, *114*, 5149-5155.
[12] Tersoff, J. Phys. Rev. Lett. 1986, *56*, 632.
[13] Hoover, W.G. Phys. Rev. A, 1985, *31*, 1695.
[14] Humphrey, W.; Dalke, A.; Schulte, K. J. Mol. Graphics. 1996, *14*, 33-38.
[15] The CP2K developers group (2010), http://cp2k.berlios.de
[16] Anderson, P. W. Phys. Rev. 1958, *109,* 1492.
[17] Stone, A. J.; Wales, D. J. Chem. Phys. Lett. 1986, *128*, 501–503.
[18] Alder, R.W.; Harvey, J.N. J. of the Am. Chem. Soc. 2004, *126*, 2490-2494.
[19] Bettinger, H.F.; Yakobson, B.I.; Scuseria, G.E. J. of the Am. Chem. Soc. 2003, *125*, 5572-5580.
[20] Zakharchenko, K. V.; Fasolino, A.; Los, J. H.; Katsnelson M. I. J. Phys. Cond. Matter 2011, *23*, 202202.
[21] Cross S.; Kuttel M.M.; Stone J.E.; Gain J.E.; J Mol Graph Model. 2009, *28*,131-139.